Journal of Quantitative Spectroscopy & Radiative Transfer 338 (2025) 109399

Contents lists available at ScienceDirect

Journal of Quantitative Spectroscopy and Radiative Transfer

journal homepage: www.elsevier.com/locate/jqsrt

MARVEL analysis of high-resolution spectra of ozone ($^{16}O_3$)

Apoorva Upadhyay [a], Tibor Furtenbacher [b], Armando N. Perri [a], Charles A. Bowesman [a], Eamon K. Conway [c], Katy L. Chubb [f], Alec Owens [a], Caitlin P. Dobney [d,a], Ella Bowen [e], Daniel Broner [e], Victor Ciobanu [e], Katherina Gelborova [e], Sam Livsey [e], Damilola Magbagbeola [e], Madhushree Manjunatha [e], Tom Mitchell [e], David Morohunfola [e], Emaan Wijayakoon [e], Sophie Winter [e], Jonathan Tennyson [a,*]

[a] Department of Physics and Astronomy, University College London, Gower Street, London WC1E 6BT, UK
[b] MTA-ELTE Complex Chemical Systems Research Group, H-1117 Budapest, Pázmány Péter sétány 1/A, Hungary
[c] Kostas Research Institute at Northeastern University, Burlington, MA, USA
[d] Department of Physics, University of Toronto, McLennan Physical Laboratories, 60 St. George Street, Toronto, ON M5S 1A7, Canada
[e] Parmiter's School, High Elms Lane, Garston, Nr. Watford, Hertfordshire, WD25 0UU, UK
[f] School of Physics, HH Wills Physics Laboratory, Tyndall Avenue, Bristol, BS8 1TL, UK

ARTICLE INFO

Keywords:
Ozone
Energy levels
Molecular data
Spectroscopic network
MARVEL

ABSTRACT

Accurate rotation-vibration (ro-vibrational) energy levels of the main isotopologue of ozone ($^{16}O_3$) in its ground electronic $\tilde{X}\,^1A_1$ state are determined by performing MARVEL (Measured Active Rotation Vibration Energy Levels) analysis on measured line positions from 29 sources of data published in scientific literature. A total of 50276 ro-vibrational transitions are considered yielding 13664 MARVEL energy levels of $^{16}O_3$ with their associated uncertainties. The maximum values of the energy and rotational angular momentum quantum number in the MARVEL dataset are 8167.33 cm^{-1} and $J = 67$ respectively. Variational nuclear motion calculations of $^{16}O_3$ energy levels are performed and subsequently used to assess and validate the MARVEL results. Comparisons with alternative data compilations based on effective Hamiltonians are also shown.

1. Introduction

Ozone ($^{16}O_3$) in the Earth's stratosphere acts as a shield from the harmful effects of ultra-violet radiation and its depletion has been a concern for many decades [1]. Tropospheric ozone is a pollutant while also being considered a contributor to the greenhouse effect [2,3]. Remote sensing instruments on satellite, airborne or ground-based platforms utilize spectroscopy to measure atmospheric ozone concentrations [4]. The accuracy of retrieved concentrations depends on the accuracy of ozone spectroscopic parameters [5] and there are several atmospheric and ozone specific databases dedicated to the compilation of these parameters such as HITRAN [6], GEISA [7] and S&MPO [8].

There have been many high-resolution spectroscopic studies of the pure rotational and rotation-vibration (ro-vibrational) spectrum of $^{16}O_3$ in the ground electronic $\tilde{X}\,^1A_1$ state [9–64]. Experimental determination of $^{16}O_3$ energy levels has been performed in several works [13–15,65–69], some of which also give empirical uncertainties for these energies. On the theoretical side, *ab-initio* variational models have been able to predict transition intensities accurately [70–72] particularly for many high intensity ro-vibrational bands of $^{16}O_3$. However, it is still very challenging for variationally calculated energy levels and line positions to reach experimental accuracy using *ab-initio* methods alone as illustrated in a study on $^{16}O_3$ by Tyuterev et al. [73] where sub 1 cm^{-1} root mean squared (RMS) deviation between predicted and experimental ro-vibrational band centers was achieved. *Ab-initio* variational calculations are often supplemented with refinement of the potential energy surface (PES) where accuracy can be improved significantly by fitting to MARVEL (Measured Active Rotation Vibration Energy Levels [74,75]) or empirical energies. The semi empirical approach of PES refinement has been applied to numerous studies including $H_2{}^{16}O$ [76,77], NH_3 [78], C_2H_4 [79], TiO [80] and $^{16}O_3$ [71] among others. Polyansky et al. [71] fitted a refined PES for $^{16}O_3$ which reproduces a set of 371 energies with a standard deviation of 0.027 cm^{-1}. A refined PES can generate accurate ro-vibrational wavefunctions which could subsequently be used to calculate line intensities with greater accuracy [76]. A particular advantage of variational calculations is that

* Corresponding author.
E-mail address: j.tennyson@ucl.ac.uk (J. Tennyson).

https://doi.org/10.1016/j.jqsrt.2025.109399
Received 29 June 2024; Received in revised form 19 February 2025; Accepted 21 February 2025
Available online 9 March 2025

they are complete so that in principle all energy levels and transitions can be calculated and used as a validating dataset.

Effective Hamiltonian (EH) models are able to predict line positions and energies more accurately than *ab-initio* variational methods [36]. Jacquemart et al. [81] created a hybrid line-list for $^{16}O_3$ containing *ab-initio* variational intensities and EH transition frequencies to remedy this limitation of *ab-initio* and semi empirical variational calculations. There are some exceptions to the usual high accuracy of EH models as explored in a study on $^{16}O_3$ by Barbe et al. [36] who describe the challenges involved in accounting for ro-vibrational resonance interactions especially at high energies. In such situations, EH transition frequencies have been replaced with experimentally measured line positions in the latest editions of the S&MPO [8] and HITRAN [6] databases for transitions of $^{16}O_3$ where EH models do not meet the target accuracy of 10^{-3} cm^{-1} [36]. The MARVEL approach is model-free and therefore does not have to be adjusted to allow for resonances.

Numerous MARVEL studies have been performed on molecules of astrophysical and terrestrial importance as part of the ExoMol [82] project including for $H_2{}^{16}O$ and its isotopologues [83–86]; NH_3 [87]; SO_2 [88]; H_2S [89] among many others. For several line lists in the ExoMol database (such as H_2CO [90,91], AlO [92] and NH_3 [93]) the computed energy levels are substituted with MARVEL ones. This substitution is used to generate MARVEL based line positions with spectroscopic accuracy as was done in a study on H_2CO by Al-Derzi et al. [90]. The inclusion of MARVEL levels in the variational line list of H_2CO yields an extra 351 183 transitions with experimental accuracy of line positions from only 16 596 non-redundant transitions [90]. Additionally MARVEL energies can be used to calculate accurate temperature dependent partition functions which could aid better predictions of ro-vibrational line intensities [94,95]. Several MARVEL based line positions and energy levels have already been incorporated into the HITRAN database with many also being considered for future updates [6].

In this study we present a MARVEL analysis of ro-vibrational line positions of $^{16}O_3$, the results of which we hope will improve the accuracy of ozone spectroscopic data. Section 2 of this paper describes the theory of our approach in this study. Section 3 gives details of the sources of data used as input for the MARVEL procedure. Section 4 presents results of MARVEL analysis and comparisons with energies obtained from the S&MPO [8] database and variationally calculated energies. Our conclusions are given in Section 5.

2. Theory

2.1. Marvel theory and procedure

In the theory of spectroscopic networks, energy levels and transitions between them are represented by nodes and edges respectively [96]. The MARVEL program is based on the theory of spectroscopic networks and it can determine the energy levels of molecules [74,75]. An input file of measured line positions, uncertainties and quantum number labels for each transition is required (see Table 4). The MARVEL program inverts line positions into energy levels by solving the matrix equation

$$\mathbf{a}\,\mathbf{X} = \mathbf{Y} \tag{1}$$

where vector $\mathbf{Y}$ contains N_t number of measured transitions, vector $\mathbf{X}$ contains E_j number of energy levels to be determined and matrix $\mathbf{a}$ has elements +1, −1 or 0 [75]. Eq. (1) can be solved by the method of weighted least-squares [74,75] to get:

$$\mathbf{A}\,\mathbf{X} = \mathbf{B} \tag{2}$$

where

$$\mathbf{A} = \mathbf{a}^T\mathbf{w}\,\mathbf{a} \quad \text{and} \quad \mathbf{B} = \mathbf{a}^T\mathbf{w}\,\mathbf{Y} \tag{3}$$

The weight matrix $\mathbf{w} = w_{ij} = \delta_{ij}^{-2}$ is introduced where δ_{ij} is the uncertainty associated with the measured transition [74,75]. In this work we use the recently implemented MARVEL4 version of the procedure which allows the uncertainties in the final energy levels to be determined as before or by using a bootstrap procedure [97] which corrects for inconsistencies between different experimental uncertainties. The bootstrap method works by randomly varying the uncertainties of line positions over a chosen number of iterations and representing the uncertainty of each MARVEL energy level by a statistical measure over these iterations. We note that use of the bootstrap method usually results in slightly increased uncertainties [97,98].

2.2. Ozone energy levels, transitions and quantum numbers

The ozone adiabatic ground electronic $\tilde{X}\,^1A_1$ state has four minima due to the complex nature of its electronic structure with interacting electronic states and the Jahn–Teller effect [99,100]. One so-called "ring" minimum corresponds to the equilateral triangle configuration. The other three identical minima, which are spectroscopically relevant and the focus of this study, reside approximately 1.34 eV lower than the "ring" minimum and correspond to "open" geometric configurations and can be characterized by the C_{2v} point group at equilibrium [100]. The three identical "open" minima are related to permutations of oxygen nuclei and could interact with each other via tunneling, however the tunneling time scales are so long that each minimum can be considered independently [101].

In the "open" minima of the ground electronic state, ozone is characterized as an asymmetric top molecule [102]. Vibrational normal mode labels of ozone are v_1, v_2, v_3 where v_1 and v_3 correspond to symmetric and anti-symmetric stretching modes of vibrations while v_2 corresponds to the bending mode. Rotational states are labeled by J, K_a and K_c where J is the rotational angular momentum quantum number while K_a and K_c give projections of J onto molecule fixed z axis (or equivalently projections onto principal axes a and c respectively) for prolate and oblate symmetric top molecules respectively. The set of quantum numbers used to uniquely label a ro-vibrational energy level of ozone are: $(v_1, v_2, v_3, J, K_a, K_c)$. Total parity (corresponding to inversion operator E^*), p (e/f rotation-less parity), q (interchange symmetry of radial basis functions corresponding to nuclear permutation operator (12)) and J are called rigorous quantum labels because their corresponding operators commute with the molecular Hamiltonian while labels v_1, v_2, v_3, K_a, K_c are approximate. Operators E^* and (12) belong to the complete nuclear permutation inversion (CNPI) C_{2v}(M) group. Irreducible representations Γ (called irrep or symmetry) of vibrational, rotational and ro-vibrational wavefunctions of $^{16}O_3$ can be deduced from Table 1 [102–104].

The nuclei of $^{16}O_3$ are bosons, and therefore due to nuclear spin statistics, the complete total internal wavefunction $\Phi_{^{16}O_3}$ obeys

$$(12)\,\Phi_{^{16}O_3} = +\Phi_{^{16}O_3} \tag{4}$$

implying that $\Phi_{^{16}O_3}$ remains unchanged upon interchange of two identical ^{16}O nuclei [103]. Since operator (12) is equivalent to operator $\hat{C}_2$ in C_{2v} point group, upon inspecting the character table in Table 1, we can see that Γ_{total} (for $\Phi_{^{16}O_3}$) is restricted to A_1 and A_2 symmetry [103]. The ground electronic state of $^{16}O_3$ belongs to symmetry A_1 ($\Gamma_{elec} = A_1$). The symmetry of the vibrational normal coordinates Q_i for $^{16}O_3$ in terms of irreducible representations is given by [105]

$$\Gamma_Q = 2A_1 \oplus B_1 \tag{5}$$

Therefore the symmetry of the vibrational wavefunctions is determined by [103]

$$\Gamma_{vib} = (A_1)^{v_1} \otimes (A_1)^{v_2} \otimes (B_1)^{v_3} \tag{6}$$

The symmetry of rotational wavefunctions Γ_{rot} is determined according to the values of rotational quantum numbers K_a and K_c as given in

Table 1
Character table of C_{2v} point group and CNPI C_{2v}(M) group for $^{16}O_3$ with symmetry classification of its vibrational, rotational and ro-vibrational wavefunctions from their approximate and rigorous quantum labels. Labels e and o/f denote even and odd values respectively. The operators given in square brackets belong to CNPI group C_{2v}(M), equivalent to their C_{2v} point group counterparts adjacent to them.

Γ	$\hat{E}$ [E]	$\hat{C}_2$ [(12)]	$\hat{\sigma}_{xz}$ [(12)*]	$\hat{\sigma}_{yz}$ [E^*]	Normal coordinate	K_a	K_c	J_{even} (p, q)	J_{odd} (p, q)
A_1	1	1	1	1	Q_1, Q_2	e	e	(e, e)	(f, e)
A_2	1	1	−1	−1		o	o	(f, o)	(e, o)
B_1	1	−1	1	−1	Q_3	o	e	(f, e)	(e, e)
B_2	1	−1	−1	1		e	o	(e, o)	(f, o)

Table 1. For ^{16}O the nuclear spin angular momentum quantum number $I = 0$ and therefore its projection onto the space-fixed Z axis $\sigma = 0$. Hence the nuclear spin function for ^{16}O nucleus is $\delta_{^{16}O} = |0, 0\rangle$. This results in only one nuclear spin wavefunction $\Phi_{ns} = \delta_{^{16}O}\delta_{^{16}O}\delta_{^{16}O}$ for $^{16}O_3$ with symmetry $\Gamma_{ns} = A_1$ [103]. Only ro-vibronic (rotation-vibration-electronic) states with symmetry A_1 and A_2 can be combined with the single nuclear spin wavefunction Φ_{ns} to produce allowed complete total internal wavefunctions $\Phi_{^{16}O_3}$ with the required symmetry $\Gamma_{total} = A_1$, A_2. This results in "missing" states of $^{16}O_3$ in the sense that half the ro-vibronational states that can be obtained with variational nuclear motion calculations do not physically exist [103].

In terms of approximate quantum numbers, the symmetry of allowed ro-vibrational energy levels in the ground electronic $\tilde{X}\,^1A_1$ state (with respect to the symmetry of allowed wavefunctions $\Phi_{^{16}O_3}$) can be determined by the quantum numbers v_3, K_a, K_c as follows: If v_3 is even, select rotational levels with $K_a + K_c$ even. If v_3 is odd, select rotational levels with $K_a + K_c$ odd. The dipole allowed transitions of $^{16}O_3$ follow the strict selection rules [102]: $A_1 \leftrightarrow A_2$, $\Delta J = 0, \pm 1$.

If we define rotation-less parities e as $p = 0$ and f as $p = 1$, then rotation-less parity in terms of rigorous quantum labels is given by the expression $(-1)^p$ with total parity (+/-) given by $(-1)^{J+p}$. We can also calculate rotation-less parity from approximate quantum numbers as follows: if $K_a + K_c = even$, then the state has e rotation-less parity; if $K_a + K_c = odd$, then the state has f rotation-less parity.

3. Experimental data sources

3.1. Overview

We searched the literature for experimentally measured ro-vibrational line positions with assigned quantum numbers (v_1, v_2, v_3, J, K_a, K_c) for upper and lower states and found many articles that contain data either in tables within the paper or as part of the supplementary information. A detailed summary of data sources used in MARVEL analysis is given in Table 2. Data from most sources was scanned, digitized (using the *FineReader OCR Pro* application) and cleaned in order to be used as input into the MARVEL program. The digitization process often led to errors in the scanned data (such as mislabeling of line positions and quantum numbers) which we corrected manually and by using the technique of combination differences implemented within the MARVEL program.

A number of transitions were not validated (and hence excluded from analysis) as indicated by the A/V column in Table 2 because these lines are considered by the MARVEL program as inconsistent with the other transitions in the network. The excluded lines are retained in the MARVEL input with a negative value for the transition frequency.

There are many sources (particularly in the energy level range 3000–6000 cm^{-1}) which we considered but could not use for MARVEL analysis because the actual measured line positions were not available. All such data sources along with their respective reasons for us being unable to include them in this work are listed in Table 3. The unavailable measurement data contributes to the incompleteness of the MARVEL dataset of ozone energies (as illustrated in Fig. 4). In these circumstances, we extract what appear to be measured line positions from the HITRAN database [6]. Extracted transitions from the HITRAN database are contained in a source labeled as MagentaSMPO, further details of which are given in the following section.

An extract from the MARVEL input file is given in Table 4. We note that the MARVEL input format has two uncertainty columns, where the first column refers to the original experimental uncertainty. The MARVEL program can change the original uncertainty of the transition, and the new uncertainty value is given in the second column; this option was not used here. The complete MARVEL input file is provided as part of the supplementary material of this article. The MARVEL program also requires a file containing a list of all sources and their units for line positions as input (this file is also provided in the supplementary section of this paper).

3.2. Notes on particular sources

Although line-by-line experimental uncertainties are preferred, they are not provided in some sources such as **11BaDeTyKa** [13] and **12DeBaStTy** [14]. In this situation, we used the generic experimental uncertainty of 0.001 cm^{-1} (as provided in the articles) for all bands in these sources. Where line-by-line uncertainties are not available, we use an overall uncertainty for all measured line positions in the experiment, where we assume the uncertainties to be generic (since the assignment of spectra is done after the measurements are collected). Consequently, for cases where we have used generic uncertainty, the input uncertainties for some transitions are likely to be underestimated.

77BaSeJoMo [21]: This data source contains many so-called "blended" lines. These are transitions that each have a unique set of quantum numbers but have the same value of the transition frequency (probably due to low resolution of the measuring apparatus). For example, the two transitions 77BaSeJoMo.874 and 77BaSeJoMo.875 are blended with the same value of line position, so the uncertainty of one of the pair (along with all such cases in this source) is increased from 0.001 cm^{-1} to 0.003 cm^{-1}.

78Lovas [110]: This source is a useful compilation of spectroscopic measurements; however we took measured line positions directly from the original sources cited in this source.

81BaSeJoGo [24]: This source only provides J and K_{-1} quantum numbers. K_{-1} is assumed to be K_a based on the notation of 77BaSeJoMo [21]. K_c can then be uniquely determined by:

$$\begin{aligned} K_c &= J - K_a \quad \text{if} \quad v_3 \quad \text{is even} \\ K_c &= J - K_a + 1 \quad \text{if} \quad v_3 \quad \text{is odd} \end{aligned} \tag{7}$$

The values of K_c for this source were calculated from Eqs (7) and subsequently used in the MARVEL input.

78MoDeBeBa [23] and **88PiCoBrRi** [28]: We encountered issues with a very large number of inconsistent lines between these sources described by the MARVEL program as "very bad" lines. The MARVEL program recommends an optimal uncertainty for every input transition and very bad lines are defined as those having the ratio of optimal and original (experimentally estimated) uncertainty between 10 and 100. We analyze common transitions between 78MoDeBeBa and 88PiCoBrRi and plot the distribution of line position differences as shown in Fig. 1(a). Assuming a normal distribution of line position differences, the standard deviation of the distribution is 0.016 cm^{-1}

Table 2
Summary and statistics of all sources of transition frequencies used in the MARVEL input.

Source	Reference	Wavenumber range	A/V	δ_{AOU}	δ_{AMR}	Ratio
01SmDeBeRi	[9]	991.61402 – 1128.75165	376/376	1.827e−05	1.207e−05	0.661
01WeDeFl	[106]	6503.66932 – 6593.61037	397/396	1.401e−03	9.077e−04	0.648
05CoBaDeMa	[10]	5.78685 – 21.97570	252/248	2.226e−06	5.506e−07	0.247
07BaDeTyKa	[11]	6225.12000 – 6395.37869	2451/2451	2.000e−03	1.815e−05	0.009
10GuMoJaCa	[12]	1132.59923 – 1134.50971	15/15	4.233e−05	1.236e−05	0.292
11BaDeTyKa	[13]	6392.75549 – 7292.60504	1320/1320	1.000e−03	1.097e−05	0.011
12DeBaStTy	[14]	7346.27000 – 7584.05051	1212/1212	1.000e−03	7.674e−06	0.008
15CaKaMoBa	[15]	7629.46367 – 7864.68990	782/782	1.500e−03	4.520e−06	0.003
17DrCrYu	[16]	23.09493 – 24.00969	7/7	1.243e−07	1.909e−09	0.015
22JaBoElJe	[107]	997.55214 – 2132.34946	816/816	3.000e−05	1.798e−05	0.599
53TrGhBuGo	[17]	1.42874 – 3.94821	4/4	7.425e−06	2.931e−06	0.395
69PoStFl	[18]	0.36934 – 0.36934	1/1	3.300e−06	4.411e−06	1.337
70TaMo	[19]	0.30278 – 2.20853	39/39	3.300e−06	9.243e−07	0.280
71LiGaCl	[20]	1.73372 – 10.53644	69/69	2.300e−05	7.645e−06	0.332
77BaSeJoMo	[21]	0.32254 – 1071.52850	1023/1020	9.629e−04	1.740e−03	1.808
77DeDuBe	[22]	0.49439 – 12.61810	111/110	3.300e−06	1.375e−06	0.417
78MoDeBeBa	[23]	0.66880 – 1046.94800	1084/1075	4.091e−02	1.070e−02	0.262
81BaSeJoGo	[24]	1006.27900 – 1218.87800	1912/1902	1.335e−02	3.069e−03	0.230
81KoHiFa	[25]	1039.32761 – 1053.91977	18/18	2.667e−04	2.292e−04	0.859
84CaDiFuTr	[26]	7.91030 – 147.43060	967/966	2.675e−04	3.092e−04	1.156
85PiCoMa	[27]	0.49439 – 1218.05960	3089/3047	6.965e−04	3.752e−04	0.539
88PiCoBrRi	[28]	0.89794 – 859.41300	3248/3237	6.078e−04	3.103e−04	0.510
92BaPlBoFl	[29]	2080.12827 – 2083.58555	10/10	7.000e−05	1.090e−04	1.557
92BeDeDiFu	[30]	50.20949 – 135.01084	63/63	2.888e−06	5.565e−07	0.193
94BaPlBoSu	[31]	1961.66095 – 2253.32424	637/637	1.000e−05	6.422e−06	0.642
96BaPL	[32]	4144.21860 – 4150.48330	55/55	7.000e−04	6.700e−04	0.957
96BaSuPlTy	[33]	4220.04140 – 4225.73790	34/34	7.000e−04	6.970e−04	0.996
96MiBaTyRe	[34]	4642.00760 – 4643.61830	30/30	6.000e−04	1.210e−03	2.016
97DeLoInNo	[35]	52.07695 – 122.81379	28/26	1.577e−06	3.376e−08	0.021
MagentaSMPO	[6,36]	16.50080 – 5569.00410	30226/29960	5.500e−04	1.496e−04	0.272

Source: Unique label for each data source.
Wavenumber range of transitions given in cm^{-1}.
A/V: total number of available lines in the input/ total number of lines validated.
δ_{AOU}: average original (experimental) uncertainty of source transitions given in cm^{-1}.
δ_{AMR}: average MARVEL reproduction of source transitions given in cm^{-1}.
Ratio = $\delta_{AMR}/\delta_{AOU}$.

Table 3
List of data sources considered but not included for MARVEL analysis.

Source	Reference	Wavenumber region (cm^{-1})	Reason
87FlCaDeRib	[37]	1000	Measured data not available
87DeFlCa	[38]	900 – 2000	Measured data not available
88RiSmFlCa	[39]	2100	Measured data not available
90SmRiDeFl	[40]	2700 – 3000	Measured data not available
90CaFlRiSm	[41]	3330	Measured data not available
90CaFlSmRi	[42]	5200	Measured data not available
90DePeFlCa	[43]	3600 – 3900	Measured data not available
91PeVaFlCa	[44]	4000	Measured data not available
90RiSmDeFl	[45]	2400	Measured data not available
93BaBoPlJa	[46]	4325	Measured data not available
93BoBaPlFl	[47]	3050	Measured data not available
93FlCaPeDe	[48]	3333	Measured data not available
94BoBaMiPl	[49]	3450	Measured data not available
95BoMiBaRe	[50]	3700	Measured data not available
95BaSuPlHa	[51]	2300 – 2600	Measured data not available
95BoBaPl	[52]	3700	Measured data not available
95BaMiTyHa	[53]	3850	Measured data not available
96FlBaCaPl	[54]	4900	Measured data not available
98BaCh	[55]	5700	Measured data not available
98ChBaTyPl	[56]	5780	Measured data not available
98BaPlTyMi	[57]	5080	Measured data not available
98BaChTyTab	[58]	5500 – 5570	Measured data not available
98BaChTyTaa	[59]	1300 – 1500	Measured data not available
98BaMiPlTy	[60]	2300 – 2600, 3050 – 3110	Measured data not available
02MiBaTy	[61]	2900 – 3400	Measured data not available
04DeBaTy	[62]	4100	Measured data not available
06SuBaDeTy	[63]	4300	Measured data not available
77DeDuBe	[22]	0.40 – 12.70	Data taken from original sources
53Hughes	[64]	–	Poor accuracy
24TyBaMaGr	[108]	0 – 300	Only calculated data given
24TaBaMiSt	[109]	0.3 – 7999.0	Measured data not available
06CaKaRoBa	[69]	6225 – 6830	Measured data not available

Table 4
Extract from the MARVEL input file for $^{16}O_3$.

$\tilde{\nu}$	δ	δ	v'_1	v'_2	v'_3	J'	K'_a	K'_c	v''_1	v''_2	v''_3	J''	K''_a	K''_c	Source
128.1211	0.0004	0.0004	0	1	0	32	17	15	0	1	0	31	16	16	88PiCoBrRi.354
128.9547	0.0004	0.0004	0	1	0	33	17	17	0	1	0	32	16	16	88PiCoBrRi.356
0.3571047	0.0000033	0.0000033	0	0	1	17	2	15	0	0	1	16	3	14	70TaMo.5

$\tilde{\nu}$: line position in cm^{-1}.
δ: uncertainty of line position in cm^{-1}.
$'$ and $''$ denote upper and lower states respectively.

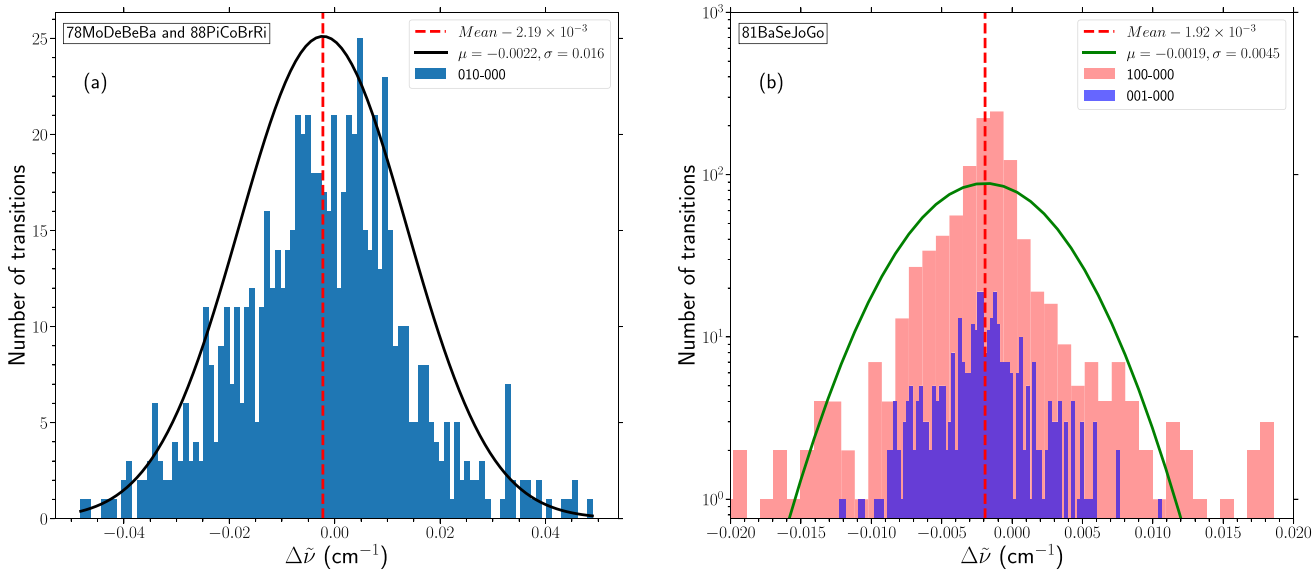

Fig. 1. Recalibration of line positions. Distribution of line position differences ($\Delta\tilde{\nu}$) of 78MoDeBeBa with 88PiCoBrRi for the 010-000 band is shown in panel (a). The distribution of line position differences of 81BaSeJoGo with all other sources in the MARVEL input for the 100-000 and 001-000 bands is shown in panel (b). The line positions are shifted (recalibrated) by an amount equal to the mean of each distribution. μ and σ in this figure are parameters of the Gaussian curves fitted to the distributions.

with the mean equal to −0.002189 cm^{-1}. We add the mean of the distribution (−0.002189 cm^{-1}) as a recalibration shift to all line positions of 78MoDeBeBa for the 010-000 band.

81BaSeJoGo [24]: A similar problem to that of 78MoDeBeBa [23] occurred for this source with the MARVEL program highlighting that the original experimental uncertainties of line positions were too small for the 001-000 and 100-000 bands. Both bands have much more recent sources of line position data so we compare 81BaSeJoGo with all the other sources in the MARVEL input for matching transitions. The distribution of line position differences is shown in Fig. 1(b) along with the combined mean of both bands. Line positions of both bands 100-000 and 001-000 for 81BaSeJoGo are recalibrated by −0.001918 cm^{-1}.

Recalibrating the transitions of 78MoDeBeBa and 81BaSeJoGo resulted in a significant reduction of very bad lines from 4086 to 2761 in the early stages of our analysis. Furthermore, by identifying and correcting errors in the scanned data, the final number of very bad lines are reduced to zero. We note that the use of the bootstrap method ensures that any issues with the underlying transitions is reflected in the uncertainty associated with the resulting energy level provided the number of transitions reaching that level (N_t) is greater than one.

MagentaSMPO [6,36]: This source is constructed because of lack of availability of measured line positions data. Empirical line position corrections from the S&MPO database [8] (line list SMPO_20d [36]) have been incorporated into the HITRAN 2020 line list for $^{16}O_3$ [6]. However, to the best of our knowledge, there does not appear to be a line-by-line labeling of empirically corrected lines in SMPO_20d and HITRAN, so we try to extract them by matching and comparing individual transitions of HITRAN 2020 line list [6] with HITRAN 2016 line list [111] for $^{16}O_3$. We try to filter out calculated lines based on the criteria that the absolute change in transition frequency (from HITRAN 2016 to HITRAN 2020) is greater than 0.0003 cm^{-1} [6]. A further comparison is performed with what appears to be a purely EH line list (SMPO_2019 [8,36]) generated from EH parameters to filter out the calculated line positions. If the transition frequency value exactly matches one in the SMPO_2019 line list, it is removed. However, it is not possible to completely filter out all calculated lines from the MagentaSMPO source because EH parameters have been updated since the release of the SMPO_2019 line list [8,36]. Therefore MagentaSMPO contains a mixture of transitions with calculated and observed line positions. Furthermore, we are unable to identify which individual lines in MagentaSMPO are observed or calculated. It will be the responsibility of future MARVEL studies on $^{16}O_3$ to ensure the identification and replacement of as many calculated lines as possible with observed ones in this source. Several lines from this source are deleted because they are inconsistent with other lines in the MARVEL input.

4. Results

Due to the uncertainty regarding the number of lines with calculated line positions in the MagentaSMPO source, there are a number of levels within the MARVEL dataset with partial or complete contributions from calculated lines. To this end, we provide the CheckTransitions.txt file in the supplementary section that provides details of individual lines that contribute to each MARVEL energy level.

4.1. The $^{16}O_3$ MARVEL network

The principal component of the MARVEL spectroscopic network of $^{16}O_3$ comprises 13,664 energy levels connected by 49,794 transitions. The MARVEL4.1 program is used to perform the calculations with

Table 5
Extract from the MARVEL energy level output file for $^{16}O_3$.

v_1	v_2	v_3	J	K_a	K_c	E_{MARVEL}	ε	N_t
0	0	0	0	0	0	0.000000000	0.000e+00	21
0	0	0	2	0	2	2.519473468	5.203e−06	53
0	0	0	1	1	1	3.948214755	3.300e−06	51
0	0	0	2	1	1	5.729320884	8.902e−06	73

E_{MARVEL}: MARVEL energy in cm^{-1}.
ε: MARVEL uncertainty of the energy level (bootstrap enabled) in cm^{-1}.
N_t: Number of transitions involving the energy level.

Cholesky decomposition chosen as the solution method. The bootstrap method of calculating MARVEL uncertainties (along with the conventional method) is implemented with 100 iterations. Both types of MARVEL energy level uncertainties are provided in the supporting information to this paper. The mean uncertainty of all MARVEL energies using the conventional method is 8.57×10^{-4} cm^{-1} while the mean uncertainty using the bootstrap method is 1.42×10^{-3} cm^{-1}. An extract of the MARVEL energy level output file is shown in Table 5. The complete output files are provided as part of the supplementary material of this article.

Table 6 shows statistics of the MARVEL dataset for ozone organized by vibrational band origins.

The MARVEL energy range extends to 8167.33 cm^{-1} with 70 vibrational states and the maximum value of the rotational angular momentum quantum number $J = 67$. Only five vibrational states with a $J = 0$ level exist in the MARVEL dataset because not many measured transitions involve levels with $J = 0$ in the MARVEL input and, of course, states with odd quanta in v_3 do not possess a $J = 0$ level. Out of a total of 29 experimental data sources considered for analysis, 19 have all their transitions validated. The $^{16}O_3$ MARVEL network is rather fragmented due to missing input data with a number of components comprising of single transitions. Transitions belonging to non principal components of the $^{16}O_3$ MARVEL network are not considered as validated.

MARVEL energy levels determined by single transitions (predominantly in the high-energy region) do not have their uncertainties adjusted by the bootstrap procedure, which means MARVEL uncertainties for these levels are likely to be underestimated; in particular, most of these transitions in the high-energy range have generic experimental uncertainties which are likely to be underestimates in some cases.

4.2. Comparison with SMPO_20d line list

MARVEL energy levels of $^{16}O_3$ are compared with energies from the SMPO_20d line list obtained from the S&MPO [8] database as shown in Fig. 2 where the energy levels are matched on quantum numbers $(v_1, v_2, v_3, J, K_a, K_c)$. In terms of line positions and energy levels, the SMPO_20d line list is based largely on EH models with empirical corrections [36]. A total of 13,476 energy levels are matched between MARVEL and SMPO_20d datasets with mean energy difference $\Delta E_{mean} = -9.52\times 10^{-4}$ cm^{-1} and standard deviation 4.40×10^{-3} cm^{-1}. While the overall agreement between the two datasets is good, cases of discrepancies are highlighted and discussed in this section. 11,116 SMPO_20d energy levels fall within the (bootstrap enabled) MARVEL uncertainty range which equates to 92.6% of all energy levels matched between the two datasets. There are 188 MARVEL energy levels that did not match on approximate quantum numbers and J with the energies from SMPO_20d.

EH models are often excellent at representing energy levels within particular ro-vibrational band(s) that they are fitted to, but can struggle with extrapolating to energies beyond that region. This has led to significant differences between MARVEL and EH treatments in previous studies [112]. EH models can also have difficulty completely accounting for ro-vibrational resonances arising from interactions between different states; for ozone these interactions are common at higher energies close to the relatively low-lying dissociation threshold of around 8500 cm^{-1} [36]. MARVEL energy levels have an advantage over EH models in that shifts due to resonances are automatically captured from measurements by the MARVEL procedure. There are many known resonance regions for $^{16}O_3$ where it is difficult to predict energy levels and line positions to experimental accuracy [36]. One such example is the 2000–3000 cm^{-1} region where vibrational states 101 and 030 interact. In particular, the (1,0,1,19,2,17) level is known to resonate with level (0,3,0,19,3,17) [36].

In the MARVEL dataset the (1,0,1,19,2,17) level is determined by sources MagentaSMPO and 22JaBoElJe whereas the (0,3,0,19,3,17) level is determined by lines only from MagentaSMPO (see the CheckTransitions.txt file available in supplementary material to this article for details of individual lines that contribute to these resonating levels). The energy difference between MARVEL and SMPO_20d for the (1,0,1,19,2,17) level in particular is substantially larger than other levels in both these vibrational states as illustrated in Fig. 3 and its inset.

Fig. 3 shows and compares the energies of interacting vibrational states for MARVEL and SMPO_20d line list with the resonant ro-vibrational levels highlighted. This resonance interaction was chosen as an illustration not because the shifts are particularly large but because of the good empirical coverage of the energy levels belonging to both vibrational states. In order to better visualize the energies of both interacting vibrational states, all MARVEL and SMPO_20d energies in Fig. 3 are shifted by prolate symmetric top ro-vibrational energies $[G_{101}+F_{101}(J, K_a)]$ of the 101 vibrational state, with rotational energies given by Eq. (9). Parameter κ_v, see Eq. (8),[103] for a particular vibrational state indicates the extent to which the energy levels of an asymmetric top molecule are correlated to prolate or oblate symmetric top energies. For vibrational states 101 and 030 of $^{16}O_3$, $\kappa_{101} = -0.97$ and $\kappa_{030} = -0.98$. Therefore all MARVEL and SMPO_20d energies in Fig. 3 are shifted by prolate symmetric top energies. The values of spectroscopic constants $A_v, B_v, C_v, \Delta_J, \Delta_{JK}$ and Δ_K are obtained from Barbe et al. [36].

$$\kappa_v = \frac{2B_v - A_v - C_v}{A_v - C_v} \tag{8}$$

$$F_{101}(J, K_a) = B_v J(J+1) + (A_v - B_v)K_a^2 - \Delta_J J^2(J+1)^2 - \Delta_{JK} J(J+1)K_a^2 - \Delta_K K_a^4 \tag{9}$$

The inset within Fig. 3 shows the difference between MARVEL and SMPO_20d energies indicating that the two datasets disagree more for one of the pair of resonating levels. As illustrated in the inset of Fig. 3, $\Delta E = -7.31\times 10^{-4}$ cm^{-1} between MARVEL and SMPO_20d for the resonant level (1,0,1,19,2,17) is significantly larger in absolute terms than $\Delta E_{mean} = -2.84 \times 10^{-6}$ cm^{-1} for the 101 vibrational state. If transitions contributing to (1,0,1,19,2,17) from MagentaSMPO have measured line positions, and if the corresponding energy from SMPO_20d is from an EH model, then Fig. 3 and its inset could be an illustration of the MARVEL algorithm being able to capture resonance shifts automatically by analyzing transitions with measured line positions, although further analysis for many more resonating levels is required which is beyond the scope of this study.

Table 6
Statistics of the MARVEL energy level dataset of $^{16}O_3$.

$v_1v_2v_3$	J range	N_{rot}	E	Mean ϵ	N_t	Data sources
000	0–67	1257	0.00–3175.39	3.02×10^{-3}	34 072	94BaPlBoSu,88PiCoBrRi,05CoBaDeMa, 10GuMoJaCa,96BaSuPlTy,81BaSeJoGo, 01SmDeBeRi,12DeBaStTy,15CaKaMoBa, 01WeDeFl,81KoHiFa,96MiBaTyRe, 92BeDeDiFu,96BaPL,92BaPlBoFl, 77DeDuBe,97DeLoInLo,85PiCoMa, 53TrGhBuGo,69PoStFl,07BaDeTyKa, MagentaSMPO,11BaDeTyKa,71LiGaCl, 17DrCrYu,22JaBoElJe,84CaDiFuTr, 77BaSeJoMo,78MoDeBeBa
001	1–64	1083	1042.91–3442.55	2.56×10^{-3}	9581	85PiCoMa,MagentaSMPO,81KoHiFa, 70TaMo,22JaBoElJe,81BaSeJoGo, 77BaSeJoMo,01SmDeBeRi
002	8–43	94	2096.54–3577.47	2.08×10^{-4}	106	94BaPlBoSu,22JaBoElJe,MagentaSMPO
003	5–62	86	3061.68–4803.52	2.39×10^{-3}	523	MagentaSMPO
004	0–53	298	4001.31–5260.42	7.49×10^{-4}	1027	MagentaSMPO
005	1–48	236	4920.00–5890.84	5.96×10^{-4}	1329	MagentaSMPO
007	5–36	35	6579.91–7072.18	1.45×10^{-3}	65	01WeDeFl
010	0–62	896	700.93–3091.06	1.33×10^{-3}	11 197	97DeLoInLo,MagentaSMPO,70TaMo, 22JaBoElJe,81BaSeJoGo,88PiCoBrRi, 78MoDeBeBa
011	2–47	253	1731.47–2613.91	1.71×10^{-3}	401	78MoDeBeBa,22JaBoElJe,MagentaSMPO
012	2–61	65	2728.55–4233.58	7.31×10^{-4}	703	MagentaSMPO
013	1–55	261	3699.10–4919.29	6.79×10^{-4}	1460	MagentaSMPO
014	5–50	247	4653.47–5756.93	5.68×10^{-4}	1585	96MiBaTyRe,MagentaSMPO
020	0–54	537	1399.27–2934.11	1.08×10^{-3}	1695	88PiCoBrRi,78MoDeBeBa,70TaMo, MagentaSMPO
022	6–52	50	3407.92–4452.58	6.12×10^{-4}	413	MagentaSMPO
023	1–47	176	4347.53–5299.77	5.84×10^{-4}	814	MagentaSMPO
025	1–40	367	6305.83–7084.36	2.01×10^{-3}	913	07BaDeTyKa
030	15–26	20	2194.20–2377.15	9.93×10^{-4}	29	MagentaSMPO
031	5–39	31	3150.45–3782.14	6.59×10^{-4}	128	MagentaSMPO
044	11–49	147	6559.12–7416.59	1.01×10^{-3}	427	11BaDeTyKa
045	2–23	53	7456.95–7673.29	1.00×10^{-3}	146	12DeBaStTy
100	0–64	993	1103.14–3638.68	2.79×10^{-3}	7611	85PiCoMa,MagentaSMPO,81KoHiFa, 22JaBoElJe,81BaSeJoGo,77BaSeJoMo, 10GuMoJaCa,01SmDeBeRi
101	1–53	357	2111.61–3378.23	2.06×10^{-4}	858	94BaPlBoSu,92BaPlBoFl,MagentaSMPO, 22JaBoElJe
102	4–63	127	3104.06–4679.96	9.75×10^{-4}	782	MagentaSMPO
103	1–60	251	4022.66–5496.54	1.13×10^{-3}	980	MagentaSMPO
104	2–34	118	4924.99–5678.23	5.73×10^{-4}	646	MagentaSMPO
110	2–46	272	1798.77–2661.98	1.05×10^{-3}	644	MagentaSMPO,81BaSeJoGo
111	2–61	156	2800.27–4434.20	8.17×10^{-4}	878	MagentaSMPO
112	2–59	213	3747.24–5146.93	6.64×10^{-4}	1623	MagentaSMPO
113	1–51	416	4659.75–5808.21	6.17×10^{-4}	2662	96MiBaTyRe,MagentaSMPO
114	8–40	24	5569.35–6164.11	5.53×10^{-4}	100	MagentaSMPO
121	3–50	84	3464.08–4655.10	6.25×10^{-4}	542	MagentaSMPO
122	10–47	106	4434.53–5257.81	5.73×10^{-4}	504	MagentaSMPO
123	1–35	112	5295.12–5926.20	6.28×10^{-4}	441	MagentaSMPO
124	14–42	31	6439.37–7021.99	2.00×10^{-3}	61	07BaDeTyKa
125	1–33	173	7131.55–7588.41	1.00×10^{-3}	443	11BaDeTyKa
130	8–37	8	3256.60–3733.06	6.31×10^{-4}	25	MagentaSMPO
131	3–39	133	4148.81–4796.44	6.43×10^{-4}	851	MagentaSMPO
132	19–32	7	5275.03–5527.85	5.53×10^{-4}	14	MagentaSMPO
153	1–25	155	7290.73–7672.57	1.00×10^{-3}	447	11BaDeTyKa
200	4–54	243	2209.52–3393.23	3.34×10^{-4}	508	94BaPlBoSu,MagentaSMPO
201	3–52	92	3219.02–4399.17	1.07×10^{-3}	507	MagentaSMPO
202	6–58	197	4170.39–5499.02	6.37×10^{-4}	669	96BaPL,MagentaSMPO
203	1–43	157	5077.88–5870.95	5.82×10^{-4}	349	MagentaSMPO
205	1–37	157	6587.77–7120.85	1.47×10^{-3}	331	01WeDeFl
210	12–55	57	2979.91–4187.40	6.63×10^{-4}	632	MagentaSMPO
211	1–47	292	3850.73–4873.83	6.24×10^{-4}	1638	MagentaSMPO
212	8–51	101	4821.46–5836.04	5.96×10^{-4}	382	MagentaSMPO
213	1–35	143	5519.60–6188.38	5.68×10^{-4}	517	MagentaSMPO
220	16–46	8	3679.25–4427.45	6.02×10^{-4}	21	MagentaSMPO
221	1–39	259	4512.15–5320.35	5.78×10^{-4}	1419	MagentaSMPO
223	1–37	284	6387.78–7100.76	2.00×10^{-3}	717	07BaDeTyKa
230	32–32	1	4688.22–4688.22	5.55×10^{-4}	2	MagentaSMPO
243	2–30	116	7691.38–8097.25	1.50×10^{-3}	271	15CaKaMoBa
271	3–26	83	7744.16–7996.29	1.50×10^{-3}	213	15CaKaMoBa

(*continued on next page*)

Table 6 (*continued*).

$v_1v_2v_3$	J range	N_{rot}	E	Mean ε	N_t	Data sources
301	2–49	202	4255.11–5206.59	6.30×10^{-4}	508	96BaSuPlTy,MagentaSMPO
310	8–50	201	4023.08–5105.27	5.93×10^{-4}	438	MagentaSMPO
311	2–42	152	4911.99–5650.03	5.68×10^{-4}	1166	MagentaSMPO
320	8–39	32	4702.10–5314.54	5.55×10^{-4}	152	96MiBaTyRe,MagentaSMPO
321	19–19	2	5719.00–5741.30	5.52×10^{-4}	6	MagentaSMPO
330	25–25	1	5630.80–5630.80	5.53×10^{-4}	4	MagentaSMPO
351	2–25	127	7461.26–7770.35	1.00×10^{-3}	369	12DeBaStTy
400	17–17	1	4547.51–4547.51	5.52×10^{-4}	6	MagentaSMPO
401	2–34	124	5312.64–5900.68	5.63×10^{-4}	279	MagentaSMPO
405	1–26	120	7863.94–8167.33	1.50×10^{-3}	298	15CaKaMoBa
430	11–35	36	6449.13–6880.48	2.00×10^{-3}	75	07BaDeTyKa
501	1–35	271	6356.53–6976.90	2.00×10^{-3}	685	07BaDeTyKa
521	1–30	122	7579.60–7966.30	1.00×10^{-3}	310	12DeBaStTy
530	15–15	1	7545.27–7545.27	1.00×10^{-3}	4	12DeBaStTy
601	1–31	153	7395.60–7891.81	1.00×10^{-3}	383	12DeBaStTy
610	13–13	1	7275.63–7275.63	1.00×10^{-3}	3	11BaDeTyKa

$v_1v_2v_3$: vibrational normal mode quantum numbers defining the vibrational state.
E: energy range of vibrational state in cm^{-1}.
Mean ε: mean of the (bootstrap enabled) MARVEL uncertainties in cm^{-1}.
N_{rot}: number of rotational levels in the vibrational state.
N_t: number of transitions involving the vibrational state.

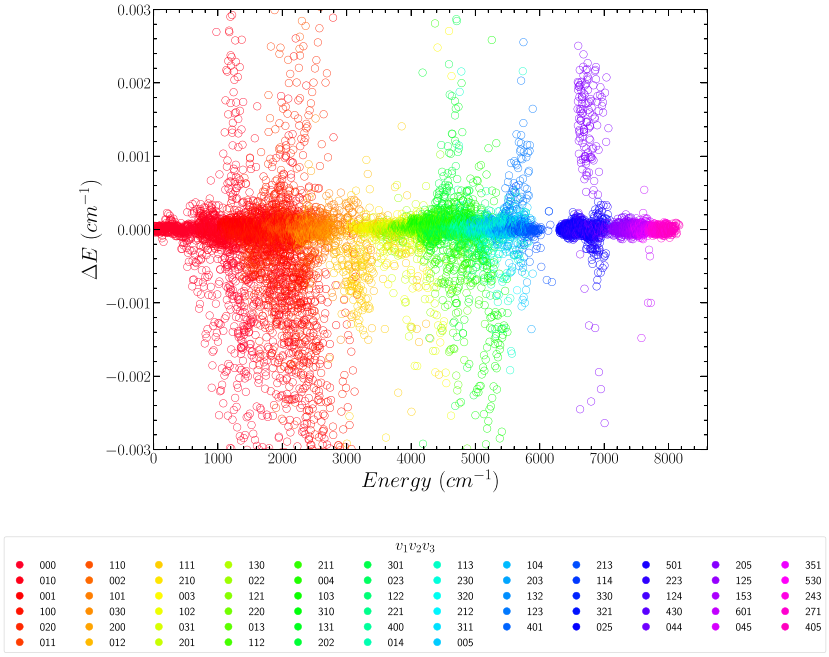

Fig. 2. Comparison of matched energy levels between MARVEL and SMPO_20d line list. ΔE is the energy difference. *Energy* on the horizontal axis gives the energy value of a ro-vibrational level. The energy levels are classified according to their vibrational band origins with legend $v_1v_2v_3$ giving the vibrational normal mode labels.

Despite extracting data from the HITRAN database to build the MagentaSMPO source, lack of availability of experimental line position data in certain spectral regions contributes to missing energy levels in the ozone MARVEL dataset. All MARVEL energy levels of ozone from this work are shown in Fig. 4.

4.3. Comparison with variational calculations

EVEREST [113] is a computational program that solves the time-independent nuclear motion Schrödinger equation variationally for triatomic molecules using an exact kinetic energy operator in a generalized coordinate system. This program is used to calculate ro-vibrational energy levels of $^{16}O_3$ in its ground electronic $\tilde{X}\,^1A_1$ state in order to verify our MARVEL analysis. The calculations are performed in Radau internal coordinates (r_1, r_2, θ) with bisector molecule fixed embedding [114]. We use 60 associated Legendre polynomials as basis functions for the angular coordinate θ with range [0°,180°] and 40 Sinc-DVR (discrete variable representation) functions as basis for the r_1 and r_2 radial coordinates with range [1.0,4.0] Å. An atomic mass of ^{16}O equal to 15.994915 Da is used in calculations which accounts very approximately for non-adiabatic effects. The dimension of the Hamiltonian in the first step of the calculation is 5000. The number of eigenvectors from the first step taken as basis functions in the second step of the calculation is equal to 4000. The resulting variational energies span up to the dissociation threshold of $^{16}O_3$ of around 8500 cm^{-1} and $J = 80$. The number of basis functions, grid size and dimensions of the Hamiltonian are varied to ensure convergence of calculated energies. The fitted potential energy surface (PES1) from Polyansky et al. [71] is used as input to EVEREST calculations in this work.

In EVEREST the symmetries of ro-vibrational levels $\Gamma_{rot-vib}$ are determined by the CNPI $C_{2v}(M)$ operators E^* and (12) (equivalent to operators $\hat{\sigma}_{yz}$ and $\hat{C}_2$ respectively in C_{2v} point group) [103]. EVEREST transforms the ro-vibrational wavefunctions under operators E^* and (12) and assigns their characters to each ro-vibrational energy level.

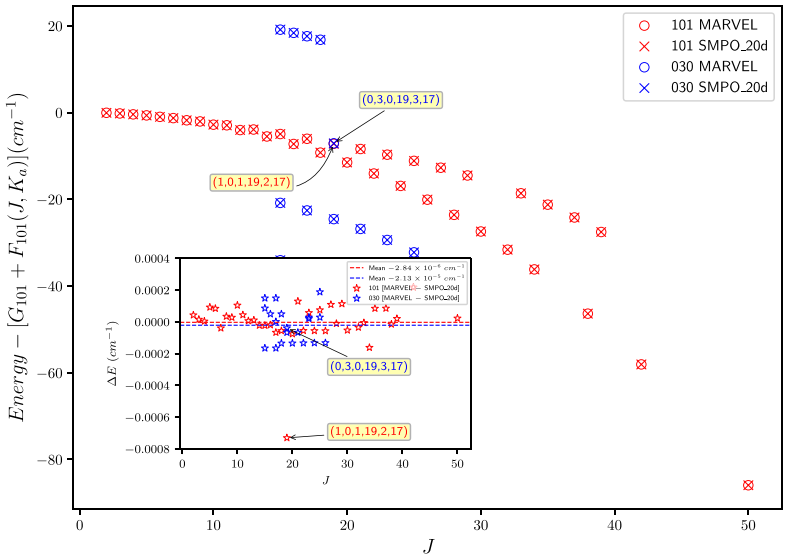

Fig. 3. MARVEL and SMPO_20d energies of two interacting vibrational states (101 and 030) are plotted against rotational angular momentum quantum number J. The resonant energy levels with quantum numbers $(v_1, v_2, v_3, J, K_a, K_c)$ are (1,0,1,19,2,17) and (0,3,0,19,3,17). The energies of MARVEL and SMPO_20d levels are shifted by prolate symmetric top energies with vibrational band origin of the 001 state G_{101} = 2110.78 cm^{-1}. The inset shows the difference between SMPO_20d and MARVEL energies (ΔE) for interacting vibrational states with resonant energy levels labeled with their respective quantum numbers.

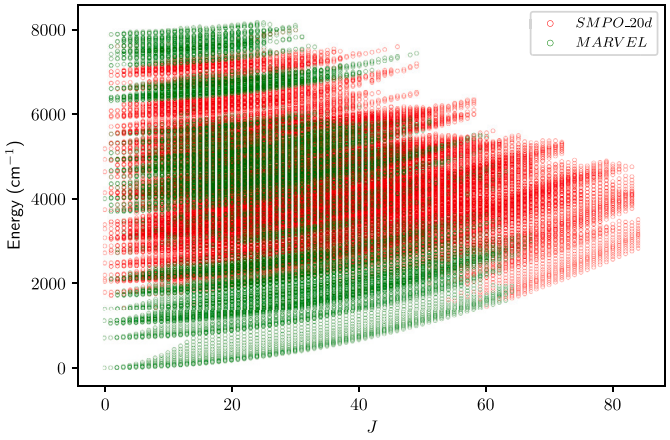

Fig. 4. Overview of all MARVEL energy levels of $^{16}O_3$. Energies obtained from the SMPO_20d linelist [8,36] are used to indicate regions where there are missing MARVEL levels.

Table 1 illustrates how we can determine $\Gamma_{rot-vib}$ of each energy level from the characters and then subsequently filter half the energy levels to retain allowed physical energies with symmetry $\Gamma_{rot-vib} = A_1, A_2$ that satisfy Eq. (4) as per the spin statistics theorem. MARVEL energy levels should automatically belong to total symmetry A_1 or A_2 if they are determined exclusively from observed line positions, however due to an unknown number of calculated lines present in MagentaSMPO, we checked the symmetries of all MARVEL levels from their approximate quantum numbers v_3, K_a and K_c using Table 1, and indeed there are no non-physical MARVEL levels with symmetry B_1 or B_2.

EVEREST energies are filtered for symmetries $\Gamma_{rot-vib} = A_1, A_2$ and subsequently matched uniquely to MARVEL energies on J, symmetry and nearest energy. The results of this comparison is shown in Fig. 5.

All MARVEL levels are uniquely matched and validated against EVEREST variational energies with ΔE_{mean} = 0.25 cm^{-1} and standard deviation 1.09 cm^{-1}. The potential energy surface PES1 from Polyansky et al. [71] performs less well at high J's as illustrated in Fig. 5(b) because it is fitted to 371 energy levels up to J = 5 and 6000 cm^{-1}. We note the *ab-initio* potential of Tyuterev et al. [73] has the correct shape and dissociation asymptote at large internuclear distances and therefore we expect it to be more accurate than PES1 above 6000 cm^{-1}. A detailed comparison of both potential energy surfaces is beyond the scope of this study but will be done in an upcoming publication currently in preparation. Systematic structures in ΔE at lower energies in Fig. 5(a) also indicate scope for improvement in the fitted PES1 potential energy surface from Polyansky et al. [71].

5. Conclusion

A total of 13,664 MARVEL ro-vibrational energy levels of the main isotopologue of ozone ($^{16}O_3$) in its ground electronic $\tilde{X}\ ^1A_1$ state up to 8167.33 cm^{-1} are derived along with their uncertainties, by analyzing 50,276 transitions from 30 data sources. 49,926 transitions are validated. Line positions of 78MoDeBeBa (band 010-000) and 81BaSeJoGo (bands 100-000 and 001-000) are recalibrated.

Unusually we were unable to obtain a substantial proportion of the measured line positions as listed in Table 3; with access to these data our results would have been even more comprehensive. However, we tried to extract as many measured line positions as possible from the HITRAN database (as empirically corrected line positions from SMPO_20d line list were incorporated into the latest version of HITRAN) by constructing the MagentaSMPO source. Extracting the empirically corrected measured lines became a complex task because (to the best of our knowledge) there does not appear to be line-by-line labeling to distinguish observed lines from calculated ones in HITRAN and SMPO_20d. Therefore MagentaSMPO source also contains an unknown number of calculated lines because we are unable to identify them and completely filter them out. As a result the MARVEL dataset suffers from a number of its levels having partial or complete contributions from calculated lines. The CheckTransitions.txt file provided as part of the supplementary material shows the contribution of individual lines for every MARVEL energy level. We hope that subsequent MARVEL studies on $^{16}O_3$ will be able to identify and replace calculated lines in MagentaSMPO by transitions with measured line positions as data availability improves in the future. At present the unavailability of experimental data makes it difficult to prove the consistency of the available data compilations.

MARVEL energies are extensively compared with SMPO_20d line list energies obtained from the S&MPO database [8] with ΔE_{mean} = -9.52×10^{-4} cm^{-1} and standard deviation 4.40 $\times$ 10^{-3} cm^{-1} for all

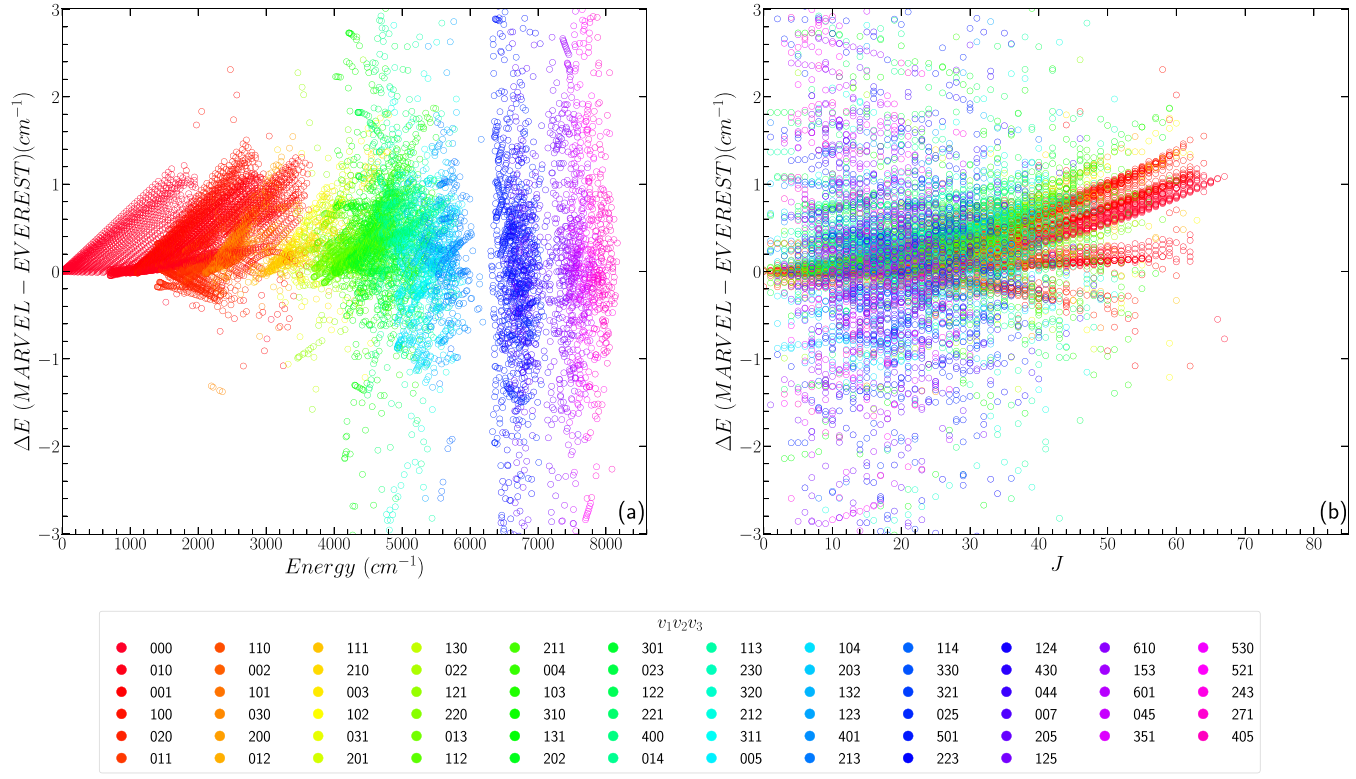

Fig. 5. Comparison of MARVEL and EVEREST energy levels. Energy levels are uniquely matched on J, symmetry and nearest energy. The energies are classified according to their vibrational band origins. The difference in energy (ΔE) is plotted as a function of energy and J in panels (a) and (b) respectively.

13,476 energy levels matched between them on approximate quantum numbers and J as shown in Fig. 2. The inset within Fig. 3 shows that MARVEL and SMPO_20d energies disagree more for the (1,0,1,19,2,17) resonant level which (providing that the MARVEL levels are determined exclusively by measured lines) perhaps illustrates the ability of the MARVEL algorithm to automatically capture resonance shifts.

The nuclear Schrödinger equation is solved variationally for $^{16}O_3$ up to the dissociation threshold and $J = 80$ using the EVEREST program [113]. All MARVEL energies are uniquely matched and validated against variationally calculated ro-vibrational energies with ΔE_{mean} = 0.25 cm^{-1} and standard deviation 1.09 cm^{-1} as shown in Fig. 5.

A small section of the spectroscopic network of $^{16}O_3$ is shown in the graphical abstract. Nodes and edges represent energy levels and spectroscopic transitions respectively. The vibrational states are represented by nodes of different colors. Each node is labeled by the unique set of quantum numbers $[v_1, v_2, v_3, J, K_a, K_c]$. The size of a node is defined as being directly proportional to the number of transitions connected to it. The largest node is the ground vibrational state involved in most transitions.

The results of this study will be used to improve the accuracy of variational line list calculations for ozone as part of the ExoMol [82] project (paper currently in preparation). A significant contribution to this study was made by the students of Parmiter's School as part of the ORBYTS project [115].

After submission of this study for publication, Tashkun et al. [109] provide a rather similar analysis giving energy levels of ozone. Their analysis is based on a more complete set of measured transitions data which, to the best of our knowledge, is not made available either in their article [109] or elsewhere.

CRediT authorship contribution statement

Apoorva Upadhyay: Writing – original draft, Visualization, Validation, Supervision, Software, Methodology, Investigation, Formal analysis, Data curation. **Tibor Furtenbacher:** Software. **Armando N. Perri:** Formal analysis. **Charles A. Bowesman:** Formal analysis. **Eamon K. Conway:** Formal analysis. **Katy L. Chubb:** Investigation. **Alec Owens:** Formal analysis. **Caitlin P. Dobney:** Investigation. **Ella Bowen:** Investigation. **Daniel Broner:** Investigation. **Victor Ciobanu:** Investigation. **Katherina Gelborova:** Investigation. **Sam Livsey:** Investigation. **Damilola Magbagbeola:** Investigation. **Madhushree Manjunatha:** Investigation. **Tom Mitchell:** Investigation. **David Morohunfola:** Investigation. **Emaan Wijayakoon:** Investigation. **Sophie Winter:** Investigation. **Jonathan Tennyson:** Writing – review & editing, Supervision, Funding acquisition, Conceptualization.

Declaration of competing interest

The authors declare no conflict of interest

Acknowledgments

We would like to thank Ben Cummings, Alastair Lavin and Neena Bush from Parmiter's School, along with William Dunn and Alice Sheppard from University College London, for their help and support. We also thank Alexander O. Mitrushchenkov from Universite Paris-Est for helpful discussions and Alain Barbe for supplying the results from Ref. [116]. This work was supported by the UK National Environment Research Council (NERC) through grant number NE/T000767/1.

Appendix A. Supplementary data

Supplementary material related to this article can be found online at https://doi.org/10.1016/j.jqsrt.2025.109399.

Data availability

All data given in the supporting material.

References

[1] Solomon S. Stratospheric ozone depletion: A review of concepts and history. Rev Geophys 1999;37:275–316.

[2] Fishman J, Bowman KW, Burrows JP, Richter A, Chance KV, Edwards DP, et al. Remote sensing of tropospheric pollution from space. Bull Am Meteorol Soc 2008;89:805–22.

[3] Worden HM, Bowman KW, Worden JR, Eldering A, Beer R. Satellite measurements of the clear-sky greenhouse effect from tropospheric ozone. Nat Geosci 2008;1:305–8.

[4] Viatte C, Schneider M, Redondas A, Hase F, Eremenko M, Chelin P, et al. Comparison of ground-based FTIR and Brewer O_3 total column with data from two different IASI algorithms and from OMI and GOME-2 satellite instruments. Atmospheric Meas Tech 2011;4:535–46.

[5] Smith MAH, Devi VM, Benner DC. The quest for ozone intensities in the 9–11 μm region: a retrospective. J Quant Spectrosc Radiat Transfer 2012;113:825–8.

[6] Gordon IE, Rothman LS, Hargreaves RJ, Hashemi R, Karlovets EV, Skinner FM, et al. The HITRAN2020 molecular spectroscopic database. J Quant Spectrosc Radiat Transfer 2020;277:107949.

[7] Delahaye T, Armante R, Scott N, Jacquinet-Husson N, Chédin A, Crépeau L, et al. The 2020 edition of the GEISA spectroscopic database. J Mol Spectrosc 2021;380:111510.

[8] Babikov YL, Mikhailenko SN, Barbe A, Tyuterev VG. S & MPO–an information system for ozone spectroscopy on the WEB. J Quant Spectrosc Radiat Transfer 2014;145:169–96.

[9] Smith MAH, Devi VM, Benner DC, Rinsland CP. Absolute intensities of $^{16}O_3$ lines in the 9–11 μm region. J Geophys Res: Atmos 2001;106.

[10] Colmont JM, Bakri B, Demaison J, Mader H, Willaert F, Tyuterev VG, et al. Microwave fourier transform, millimeterwave, and submillimeterwave spectra of ozone in its vibrational ground state. J Mol Spectrosc 2005;233:293–6. http://dx.doi.org/10.1016/j.jms.2005.06.017.

[11] Barbe A, De Backer-Barilly MR, Tyuterev VG, Kassi S, Campargue A. CW-cavity ring down spectroscopy of the ozone molecule in the 6220-6400 cm^{-1} region. J Mol Spectrosc 2007;246:22–38. http://dx.doi.org/10.1016/j.jms.2007.08.001.

[12] Guinet M, Mondelain D, Janssen C, Camy-Peyret C. Laser spectroscopic study of ozone in the 100 ← 000 band for the SWIFT instrument. J Quant Spectrosc Radiat Transfer 2010;111:961–72.

[13] Barbe A, De Backer-Barilly MR, Tyuterev VG, Kassi S, Campargue A. Detection and analysis of new bands of $^{16}O_3$ by CRDS between 6500 and 7300 cm^{-1}. J Mol Spectrosc 2011;269:175–86. http://dx.doi.org/10.1016/j.jms.2011.06.005.

[14] De Backer M-R, Barbe A, Starikova E, Tyuterev VG, Kassi S, Campargue A. Detection and analysis of four new bands in CRDS $^{16}O_3$ spectra between 7300 and 7600 cm^{-1}. J Mol Spectrosc 2012;272:43–50. http://dx.doi.org/10.1016/j.jms.2012.01.001.

[15] Campargue A, Kassi S, Mondelain D, Barbe A, Starikova E, De Backer M-R, et al. Detection and analysis of three highly excited vibrational bands of $^{16}O_3$ by CW-CRDS near the dissociation threshold. J Quant Spectrosc Radiat Transfer 2015;152:84–93.

[16] Drouin BJ, Crawford TJ, Yu S. Validation of ozone intensities at 10 μm with thz spectrometry. J Quant Spectrosc Radiat Transfer 2017;203:282–92.

[17] Trambarulo R, Ghosh SN, Burrus Jr CA, Gordy W. The molecular structure, dipole moment, and g factor of ozone from its microwave spectrum. J Chem Phys 1953;21:851–5.

[18] Pochan JM, Stone RG, Flygare WH. Molecular g values, magnetic susceptibilities, molecular quadrupole moments, and second moments of the electronic charge distribution in OF_2, O_3, and SO_2. J Chem Phys 1969;51:4278–86.

[19] Tanaka T, Morino Y. Coriolis interaction and anharmonic potential function of ozone from the microwave spectra in the excited vibrational states. J Mol Spectrosc 1970;33:538–51.

[20] Lichtenstein M, Gallagher JJ, Clough SA. Millimeter wave spectrum of ozone. J Mol Spectrosc 1971;40. http://dx.doi.org/10.1016/0022-2852(71)90003-8, 10+.

[21] Barbe A, Secroun C, Jouve P, Monnanteuil N, Depannemaecker JC, Duterage B, et al. IR and microwave high-resolution spectrum of ν_3-band of ozone. J Mol Spectrosc 1977;64:343–64. http://dx.doi.org/10.1016/0022-2852(77)90221-1.

[22] Depannemaecker MJC, Duterage B, Bellet MJ. Systematic calculations of rotational spectra of normal and substituted (^{18}O in place of ^{16}O) ozone molecules. J Quant Spectrosc Radiat Transfer 1977;17:519–30.

[23] Monnanteuil N, Depannemaecker JC, Bellet J, Barbe A, Secroun C, Jouve P, et al. Microwave and infrared study of ν_2 state of $^{16}O_3$ and identification of $(\nu_3 + \nu_2) - \nu_2$ band lines at 10 μm. J Mol Spectrosc 1978;71:399–413. http://dx.doi.org/10.1016/0022-2852(78)90093-0.

[24] Barbe A, Secroun C, Jouve P, Goldman A, Murcray DG. High-resolution infrared atmospheric spectra of ozone in the 10-μm region: Analysis of ν_1 and ν_3 bands-assignment of the $(\nu_1 + \nu_2)$- ν_2 band. J Mol Spectrosc 1981;86:286–97.

[25] Kostiuk T, Hillman JJ, Faris JL. Precision heterodyne measurements of ozone spectral-lines near 9.5-μm. J Mol Spectrosc 1981;89:397–404. http://dx.doi.org/10.1016/0022-2852(81)90032-1.

[26] Carlotti M, DiLonardo G, Fusina L, Trombetti A, Bonetti A, Carli B, et al. The high-resolution spectrum of ozone between 8 and 150 cm^{-1}. J Mol Spectrosc 1984;107:84–93. http://dx.doi.org/10.1016/0022-2852(84)90267-4.

[27] Pickett HM, Cohen EA, Margolis JS. The infrared and microwave spectra of ozone for the (0, 0 0), (1, 0 0), and (0, 0 1) states. J Mol Spectrosc 1985;110:186–214.

[28] Pickett HM, Cohen EA, Brown LR, Rinsland CP, Smith MAH, Devi VM, et al. The vibrational and rotational spectra of ozone for the (0, 1 0) and (0, 2 0) states. J Mol Spectrosc 1988;128:151–71.

[29] Barbe A, Plateaux JJ, Bouazza S, Flaud J-M, Camy-Peyret C. Spectral properties of ozone in the 5 μm region. J Quant Spectrosc Radiat Transfer 1992;48:599–610.

[30] Bellini M, DeNatale P, DiLonardo G, Fusina L, Inguscio M, Prevedelli M. Tunable far infrared-spectroscopy of $^{16}O_3$ ozone. J Mol Spectrosc 1992;152:256–9. http://dx.doi.org/10.1016/0022-2852(92)90136-C.

[31] Barbe A, Plateaux JJ, Bouazza S, Sulakshina O, Mikhailenko S, Tyuterev VI, et al. Experimental and theoretical study of absolute intensities of ozone spectral lines in the range 1850–2300 cm^{-1}. J Quant Spectrosc Radiat Transfer 1994;52:341–55.

[32] Barbe A, Plateaux JJ. Analysis of the $2\nu_1 + 2\nu_3$ band of ozone: Line positions and intensities. J Quant Spectrosc Radiat Transfer 1996;55:449–55.

[33] Barbe A, Sulakshina O, Plateaux JJ, Tyuterev VG, Bouazza S. Line positions and intensities of the $3\nu_1 + \nu_3$ band of ozone. J Mol Spectrosc 1996;175:296–302.

[34] Mikhailenko S, Barbe A, Tyuterev VG, Regalia L, Plateaux J. Line positions and intensities of the $\nu_1 + \nu_2 + 3\nu_3$, $\nu_2 + 4\nu_3$, and $3\nu_1 + 2\nu_2$ bands of ozone. J Mol Spectrosc 1996;180:227–35. http://dx.doi.org/10.1006/jmsp.1996.0246.

[35] DeNatale P, Lorini L, Inguscio M, Nolt IG, Park JH, DiLonardo G, et al. Accurate frequency measurements for H_2O and $^{16}O_3$ in the 119 cm^{-1} OH atmospheric window. Appl Opt 1997;36:8526–32. http://dx.doi.org/10.1364/AO.36.008526.

[36] Barbe A, Mikhailenko S, Starikova E, Tyuterev V. Infrared spectra of $^{16}O_3$ in the 900-5600 cm^{-1} range revisited: Empirical corrections to the S & MPO and HITRAN2020 line lists. J Quant Spectrosc Radiat Transfer 2021;276:107936.

[37] Flaud J-M, Camy-Peyret C, Devi VM, Rinsland CP, Smith MAH. The ν_1 and ν_3-bands of $^{16}O_3$ - line positions and intensities. J Mol Spectrosc 1987;124:209–17. http://dx.doi.org/10.1016/0022-2852(87)90135-4.

[38] Devi VM, Flaud J-M, Camy-Peyret C. Line positions and intensities for the $\nu_1+\nu_2$ and $\nu_2 + \nu_3$ bands of $^{16}O_3$. J Mol Spectrosc 1987;125:174–83.

[39] Rinsland CP, Smith MAH, Flaud J-M, Camy-Peyret C, Devi VM. Line positions and intensities of the $2\nu_3$, $\nu_1 + \nu_3$, and $2\nu_1$ bands of $^{16}O_3$. J Mol Spectrosc 1988;130:204–12. http://dx.doi.org/10.1016/0022-2852(88)90293-7.

[40] Smith MAH, Rinsland CP, Devi VM, Flaud JM, Camy-Peyret C, Barbe A. The 3.6 μm region of ozone - line positions and intensities. J Mol Spectrosc 1990;139:171–81. http://dx.doi.org/10.1016/0022-2852(90)90249-P.

[41] Camy-Peyret C, Flaud JM, Rinsland CP, Smith MAH, Devi VM, Goldman A. Line parameters for ozone hot bands in the 4.8 μm spectral region. J Mol Spectrosc 1990;139:353–60. http://dx.doi.org/10.1016/0022-2852(90)90072-X.

[42] Camy-Peyret C, Flaud JM, Smith MAH, Rinsland CP, Devi VM, Plateaux JJ, et al. The 3.3 μm bands of ozone - line positions and intensities. J Mol Spectrosc 1990;141:134–44. http://dx.doi.org/10.1016/0022-2852(90)90283-V.

[43] Devi VM, Perrin A, Flaud J-M, Camy-Peyret C, Rinsland CP, Smith MAH. Line positions and intensities for the $\nu_2 + 3\nu_3$ band of $^{16}O_3$ around 2.7 μm. J Mol Spectrosc 1990;143:381–8.

[44] Perrin A, Vasserot AM, Flaud J-M, Camy-Peyret C, Devi VM, Smith MAH, et al. The 2.5 μm bands of ozone - line positions and intensities. J Mol Spectrosc 1991;149:519–29. http://dx.doi.org/10.1016/0022-2852(91)90307-V.

[45] Rinsland CP, Smith MAH, Devi VM, Flaud JM, Camy-Peyret C. The $2\nu_2+\nu_3$ and $2\nu_2+\nu_1$ bands of $^{16}O_3$ at 4.1 μm - line positions and intensities. J Mol Spectrosc 1990;139:343–52. http://dx.doi.org/10.1016/0022-2852(90)90071-W.

[46] Barbe A, Bouazza S, Plateaux JJ, Jacon M. The $3\nu_3 + 2\nu_2$ band of ozone - line positions and intensities. J Mol Spectrosc 1993;162:335–41. http://dx.doi.org/10.1006/jmsp.1993.1288.

[47] Bouazza S, Barbe A, Plateaux JJ, Flaud J-M, Camy-Peyret C. The $3\nu_1$ and $\nu_1 + 3\nu_3 - \nu_2$ absorption-bands of $^{16}O_3$. J Mol Spectrosc 1993;160:371–7. http://dx.doi.org/10.1006/jmsp.1993.1184.

[48] Flaud J-M, Camy-Peyret C, Perrin A, Devi VM, Barbe A, Bouazza S, et al. Line parameters for ozone hot bands in the 3.3 μm spectral region. J Mol Spectrosc 1993;160:378–86. http://dx.doi.org/10.1006/jmsp.1993.1185.

[49] Bouazza S, Barbe A, Mikhailenko S, Plateaux JJ. Line positions and intensities of the $\nu_1+2\nu_2+\nu_3$ and $2\nu_2+2\nu_3$ bands of $^{16}O_3$. J Mol Spectrosc 1994;166:365–71. http://dx.doi.org/10.1006/jmsp.1994.1201.

[50] Bouazza S, Mikhailenko S, Barbe A, Regalia L, Tyuterev VG, Plateaux JJ. The $\nu_1 + \nu_2 + 2\nu_3$ and $\nu_2 + 3\nu_3$ bands of $^{16}O_3$. J Mol Spectrosc 1995;174:510–9. http://dx.doi.org/10.1006/jmsp.1995.0019.

[51] Barbe A, Sulakshina O, Plateaux JJ, Hamdouni A, Bouazza S. High-resolution infrared-spectra of ozone in the 2300-2600 cm^{-1} region. J Mol Spectrosc 1995;170:244–50. http://dx.doi.org/10.1006/jmsp.1995.1068.

[52] Bouazza S, Barbe A, Plateaux JJ. Line positions and intensities for the $2\nu_1+\nu_2+\nu_3$ band of $^{16}O_3$. J Mol Spectrosc 1995;171:86–90. http://dx.doi.org/10.1006/jmsp.1995.1103.

[53] Barbe A, Mikhailenko S, Tyuterev V, Hamdouni A, Plateaux JJ. Analysis of the $2\nu_1 + 2\nu_2 + \nu_3$ band of ozone. J Mol Spectrosc 1995;171:583–8. http://dx.doi.org/10.1006/jmsp.1995.1147.

[54] Flaud JM, Barbe A, Camy-Peyret C, Plateaux JJ. High resolution analysis of the $5\nu_3$, $3\nu_1 + \nu_2 + \nu_3$, and $\nu_1 + 4\nu_3$, bands of $^{16}O_3$: Line positions and intensities. J Mol Spectrosc 1996;177:34–9. http://dx.doi.org/10.1006/jmsp.1996.0114.

[55] Barbe A, Chichery A. The $2\nu_1 + \nu_2 + 3\nu_3$ band of $^{16}O_3$: Line positions and intensities. J Mol Spectrosc 1998;192:102–10. http://dx.doi.org/10.1006/jmsp.1998.7683.

[56] Chichery A, Barbe A, Tyuterev VG, Plateaux JJ. Analysis of high resolution measurements of the $\nu_1 + 5\nu_3$ band of ozone: Coriolis interactions with the $6\nu_3$ and $3\nu_1 + \nu_2 + 2\nu_3$ bands. Mol Phys 1998;94:751–7. http://dx.doi.org/10.1080/002689798167593.

[57] Barbe A, Plateaux JJ, Tyuterev VG, Mikhailenko S. Analysis of high resolution measurements of the $2\nu_1 + 3\nu_3$ band of ozone: Coriolis interaction with the $\nu_1 + 3\nu_2 + 2\nu_3$ band. J Quant Spectrosc Radiat Transfer 1998;59:185–94. http://dx.doi.org/10.1016/S0022-4073(97)00117-9.

[58] Barbe A, Chichery A, Tyuterev VG, Taskhun SA, Mikhailenko SN. Infrared high-resolution spectra of ozone in the range 5500-5570 cm^{-1}: analysis of $\nu_2 + 5\nu_3$ and $\nu_1 + \nu_2 + 4\nu_3$ bands. J Phys B: At Mol Opt Phys 1998;31:2559–69. http://dx.doi.org/10.1088/0953-4075/31/11/017.

[59] Barbe A, Chichery A, Tyuterev VG, Taskhun S, Mikhailenko S. The $2\nu_2$ and $3\nu_2 - \nu_2$ bands of ozone. Spectra Chim Acta A 1998;54:1935–45. http://dx.doi.org/10.1016/S1386-1425(98)00156-5.

[60] Barbe A, Mikhailenko S, Plateaux JJ, Tyuterev VG. First study of the $\upsilon_2 = 3$ dyad {(130), (031)} of ozone through the analysis of hot bands in the 2300-2800 cm^{-1} region. J Mol Spectrosc 1998;187:70–4. http://dx.doi.org/10.1006/jmsp.1997.7483.

[61] Mikhailenko S, Barbe A, Tyuterev VG. Extended analysis of line positions and intensities of ozone bands in the 2900-3400 cm^{-1} region. J Mol Spectrosc 2002;215:29–41. http://dx.doi.org/10.1006/jmsp.2002.8597.

[62] De Backer-Barilly MR, Barbe A, Tyuterev VG. First observation of the $3\nu_1 + 2\nu_3 - \nu_3$ band of $^{16}O_3$: problem of consistency between cold and hot band intensities. Mol Phys 2004;102:1707–16. http://dx.doi.org/10.1080/00268970412331287061.

[63] Sulakshina ON, Barbe A, Backer-Barilly M-RD, Tyuterev VG. Analysis of the 4300 cm^{-1} region of ozone: interactions between 122 and 023 states. In: Y. n. ponomarev and s. n. mikhailenko and l. n. sinitsa. 15th symposium on high-resolution molecular spectroscopy, vol. 6580, International Society for Optics and Photonics, SPIE; 2006, p. 28–34. http://dx.doi.org/10.1117/12.724778.

[64] Hughes RH. The microwave spectrum and structure of ozone. J Chem Phys 1953;21:959–60.

[65] Campargue A, Barbe A, De Backer-Barilly MR, Tyuterev VG, Kassi S. The near infrared spectrum of ozone by CW-cavity ring down spectroscopy between 5850 and 7000 cm^{-1}: new observations and exhaustive review. Phys Chem Chem Phys 2008;10:2925–46. http://dx.doi.org/10.1039/b719773j.

[66] Barbe A, De Backer-Barilly M-R, Tyuterev VG, Campargue A, Romanini D, Kassi S. CW-cavity ring down spectroscopy of the ozone molecule in the 5980–6220 cm^{-1} region. J Mol Spectrosc 2007;242:156–75.

[67] Kassi S, Campargue A, De Backer-Barilly M-R, Barbe A. The $\nu_1 + 3\nu_2 + 3\nu_3$ and $4\nu_1 + \nu_2 + \nu_3$ bands of ozone by CW-cavity ring down spectroscopy between 5900 and 5960 cm^{-1}. J Mol Spectrosc 2007;244:122–9.

[68] Vasilchenko S, Barbe A, Starikova E, Kassi S, Mondelain D, Campargue A, et al. Detection and assignment of ozone bands near 95% of the dissociation threshold: Ultrasensitive experiments for probing potential energy function and vibrational dynamics. Phys Rev A 2020;102:052804.

[69] Campargue A, Kassi S, Romanini D, Barbe A, De Backer-Barilly M-R, Tyuterev VG. CW-cavity ring down spectroscopy of the ozone molecule in the 6625–6830 cm^{-1} region. J Mol Spectrosc 2006;240:1–13.

[70] Tyuterev VG, Kochanov RV, Tashkun SA. Accurate ab initio dipole moment surfaces of ozone: First principle intensity predictions for rotationally resolved spectra in a large range of overtone and combination bands. J Chem Phys 2017;146:064304.

[71] Polyansky OL, Zobov NF, Mizus II, Kyuberis AA, Lodi L, Tennyson J. Potential energy surface, dipole moment surface and the intensity calculations for the 10 μm, 5 μm and 3 μm bands of ozone. J Quant Spectrosc Radiat Transfer 2018;210:127–35.

[72] Tyuterev VG, Barbe A, Jacquemart D, Janssen C, Mikhailenko SN, Starikova EN. Ab initio predictions and laboratory validation for consistent ozone intensities in the MW, 10 and 5 μm ranges. J Chem Phys 2019;150:184303.

[73] Tyuterev VG, Kochanov RV, Tashkun SA, Holka F, Szalay PG. New analytical model for the ozone electronic ground state potential surface and accurate ab initio vibrational predictions at high energy range. J Chem Phys 2013;139:134307.

[74] Furtenbacher T, Császár AG, Tennyson J. MARVEL: measured active rotational–vibrational energy levels. J Mol Spectrosc 2007;245:115–25.

[75] Furtenbacher T, Csaszar AG. MARVEL: measured active rotational–vibrational energy levels. II. Algorithmic improvements. J Quant Spectrosc Radiat Transfer 2012;113:929–35.

[76] Mizus II, Kyuberis AA, Zobov NF, Makhnev VY, Polyansky OL, Tennyson J. High-accuracy water potential energy surface for the calculation of infrared spectra. Philos Trans R Soc A: Math Phys Eng Sci 2018;376:20170149.

[77] Conway EK, Gordon IE, Tennyson J, Polyansky OL, Yurchenko SN, Chance K. A semi-empirical potential energy surface and line list for $H_2{}^{16}O$ extending into the near-ultraviolet. Atmos Chem Phys 2020;20:10015–27.

[78] Coles PA, Ovsyannikov RI, Polyansky OL, Yurchenko SN, Tennyson J. Improved potential energy surface and spectral assignments for ammonia in the near-infrared region. J Quant Spectrosc Radiat Transfer 2018;219:199–212.

[79] Mant BP, Yachmenev A, Tennyson J, Yurchenko SN. Exomol molecular line lists–XXVII. Spectra of C_2H_4. Mon Not R Astron Soc 2018;478:3220–32.

[80] McKemmish LK, Masseron T, Hoeijmakers HJ, Pérez-Mesa V, Grimm SL, Yurchenko SN, et al. Exomol molecular line lists–xxxiii. The spectrum of titanium oxide. Mon Not R Astron Soc 2019;488:2836–54.

[81] Jacquemart D, Makhnev VY, Zobov NF, Tennyson J, Polyansky OL. Synthesis of ab initio and effective hamiltonian line lists for ozone. J Quant Spectrosc Radiat Transfer 2021;269:107651.

[82] Tennyson J, Yurchenko SN, Zhang J, Bowesman CA, Brady RP, Buldyreva J, et al. The 2024 release of the ExoMol database: molecular line lists for exoplanet and other hot atmospheres. J Quant Spectrosc Radiat Transfer 2024;326:109083. http://dx.doi.org/10.1016/j.jqsrt.2024.109083.

[83] Tennyson J, Bernath PF, Brown LR, Campargue A, Császár AG, Daumont L, et al. A database of water transitions from experiment and theory (IUPAC technical report). Pure Appl Chem 2014;86:71–83. http://dx.doi.org/10.1515/pac-2014-5012.

[84] Furtenbacher T, Tóbiás R, Tennyson J, Polyansky OL, Császár AG. W2020: A database of validated rovibrational experimental transitions and empirical energy levels of $H_2^{16}O$. J Phys Chem Ref Data 2020;49:033101. http://dx.doi.org/10.1063/5.0008253.

[85] Furtenbacher T, Tóbiás R, Tennyson J, Polyansky OL, Kyuberis AA, Ovsyannikov RI, et al. W2020: A database of validated rovibrational experimental transitions and empirical energy levels part II. $H_2^{17}O$ and $H_2^{18}O$ with an update to $H_2^{16}O$. J Phys Chem Ref Data 2020;49:043103. http://dx.doi.org/10.1063/5.0030680.

[86] Furtenbacher T, Tóbiás R, Tennyson J, Gamache RR, Császár AG. Critical analysis and interpretation of experimental rovibrational transitions: The W2024 database of the water isotopologue $H_2{}^{16}O$. Sci Data 2024;11:1058. http://dx.doi.org/10.1038/s41597-024-03847-3.

[87] Furtenbacher T, Coles PA, Tennyson J, Yurchenko SN, Yu S, Drouin B, et al. Empirical rovibrational energy levels of ammonia up to 7500 cm^{-1}. J Quant Spectrosc Radiat Transfer 2020;251:107027.

[88] Tóbiás R, Furtenbacher T, Császár AG, Naumenko OV, Tennyson J, Flaud J-M, et al. Critical evaluation of measured rotational–vibrational transitions of four sulphur isotopologues of $S^{16}O_2$. J Quant Spectrosc Radiat Transfer 2018;208:152–63.

[89] Chubb KL, Naumenko O, Keely S, Bartolotto S, Macdonald S, Mukhtar M, et al. MARVEL analysis of the measured high-resolution rovibrational spectra of $h_2{}^{32}s$. J Quant Spectrosc Radiat Transfer 2018;218:178–86.

[90] Al-Derzi AR, Yurchenko SN, Tennyson J, Melosso M, Jiang N, Puzzarini C, et al. An improved rovibrational linelist of formaldehyde, $H_2{}^{12}C^{16}O$. J Quant Spectrosc Radiat Transfer 2021;266:107563. http://dx.doi.org/10.1016/j.jqsrt.2021.107563.

[91] Germann M, Hjalten A, Tennyson J, Yurchenko SN, Gordon IE, Pett C, et al. Optical frequency comb Fourier transform spectroscopy of formaldehyde in the 1250 to 1390 cm^{-1} range: experimental line list and MARVEL analysis. J Quant Spectrosc Radiat Transfer 2024;312:108782. http://dx.doi.org/10.1016/j.jqsrt.2023.108782.

[92] Bowesman CA, Shuai M, Yurchenko SN, Tennyson J. A high-resolution line list for AlO. Mon Not R Astron Soc 2021;508:3181–93.

[93] Coles PA, Yurchenko SN, Tennyson J. Exomol molecular line lists–XXXV. A rotation-vibration line list for hot ammonia. Mon Not R Astron Soc 2019;490:4638–47.

[94] Vidler M, Tennyson J. Accurate partition function and thermodynamic data for water. J Chem Phys 2000;113:9766–71.

[95] Furtenbacher T, Szabó I, Császár AG, Bernath PF, Yurchenko SN, Tennyson J. Experimental energy levels and partition function of the $^{12}C_2$ molecule. Astrophys J Suppl 2016;224:44. http://dx.doi.org/10.3847/0067-0049/224/2/44.

[96] Császár AG, Furtenbacher T. Spectroscopic networks. J Mol Spectrosc 2011;266:99–103.

[97] Tennyson J, Furtenbacher T, Yurchenko SN, Császár AG. Empirical rovibrational energy levels for nitrous oxide. J Quant Spectrosc Radiat Transfer 2024;316:108902. http://dx.doi.org/10.1016/j.jqsrt.2024.108902.

[98] Xu E, Tennyson J. Empirical rovibrational energy levels for carbonyl sulphide. Mol Phys 2024;122:e2279694. http://dx.doi.org/10.1080/00268976.2023.2279694.

[99] Alijah A, Lapierre D, Tyuterev V. Non-adiabatic coupling in the ozone molecule. Mol Phys 2018;116:2660–70.

[100] Kokoouline V, Lapierre D, Alijah A, Tyuterev V. Localized and delocalized bound states of the main isotopologue $^{48}O_3$ and of ^{18}O-enriched $^{50}O_3$ isotopomers of the ozone molecule near the dissociation threshold. Phys Chem Chem Phys 2020;22:15885–99.
[101] Tannor DJ. Jahn-Teller effects in the photodissociation of ozone. J Am Chem Soc 1989;111:2772–6.
[102] Flaud J-M, Bacis R. The ozone molecule: infrared and microwave spectroscopy. Spectrochim Acta Part A: Mol Spectrosc 1998;54:3–16.
[103] Bunker PR, Jensen P. Fundamentals of molecular symmetry. CRC Press; 2018.
[104] Underwood D. Variationally computed line lists for SO_2 and SO_3 [Ph.D. thesis], UCL (University College London); 2017.
[105] Teplukhin A. Theoretical study of ozone forming recombination reaction and anomalous isotope effect associated with it [Ph.D. thesis], Marquette University; 2017.
[106] Wenz H, Demtröder W, Flaud J. Highly sensitive absorption spectroscopy of the ozone molecule around 1.5 μm. J Mol Spectrosc 2001;209:267–77.
[107] Jacquemart D, Boursier C, Elandaloussi H, Jeseck P, Té Y, Janssen C. Multi-spectral investigation of ozone: Part II. Line intensity measurements at one percent accuracy around 5 μm and 10 μm. J Quant Spectrosc Radiat Transfer 2022;279:108050.
[108] Tyuterev VG, Barbe A, Manceron L, Grouiez B, Tashkun SA, Burgalat J, et al. Ozone spectroscopy in the terahertz range from first high-resolution synchrotron SOLEIL experiments combined with far-infrared measurements and ab initio intensity calculations. Spectrochim Acta Part A: Mol Biomol Spectrosc 2024;305:123456.
[109] Tashkun S, Barbe A, Mikhailenko S, Starikova E, Tyuterev V. Complete Ritz set of ro-vibrational energy levels of $^{16}O)_3$ deduced from experimental spectra: Critical analysis of transition frequencies in spectroscopic databases. J Phys Chem Ref Data 2024;53.
[110] Lovas FJ. Microwave spectral tables II. Triatomic molecules. J Phys Chem Ref Data 1978;7:1445–750.
[111] Gordon IE, Rothman LS, Hill C, Kochanov RV, Tan Y, Bernath PF, et al. The HITRAN2016 molecular spectroscopic database. J Quant Spectrosc Radiat Transfer 2017;203:3–69.
[112] Furtenbacher T, Coles PA, Tennyson J, Yurchenko SN, Yu S, Drouin B, et al. Empirical rovibational energy of ammonia up to 7500 cm^{-1}. J Quant Spectrosc Radiat Transfer 2020;251:107027. http://dx.doi.org/10.1016/j.jqsrt.2020.107027.
[113] Mitrushchenkov AO. A new general Renner-Teller (including $\epsilon \geq 1$) spectroscopic formalism for triatomic molecules. J Chem Phys 2012;136:024108.
[114] Sarka J, Poirier B, Szalay V, Császár AG. On neglecting Coriolis and related couplings in first-principles rovibrational spectroscopy: Considerations of symmetry, accuracy, and simplicity. II. Case studies for H_2O isotopologues, H_3^+, O_3, and NH_3. Spectrochim Acta Part A: Mol Biomol Spectrosc 2021;250:119164.
[115] Sousa-Silva C, McKemmish LK, Chubb KL, Gorman MN, Baker JS, Barton EJ, et al. Original research by young Twinkle students (ORBYTS): when can students start performing original research? Phys Educ 2017;53:015020.
[116] Barbe A, Plateaux JJ, Mikhailenko S, Tyuterev VG. Infrared spectrum of ozone in the 4600 and 5300 cm^{-1} regions: High order accidental resonances through the analysis of $\nu_1 + 2\nu_2 + 3\nu_3 - \nu_2$, $\nu_1 + 2\nu_2 + 3\nu_3$, and $4\nu_1 + \nu_3$ bands. J Mol Spectrosc 1997;185:408–16. http://dx.doi.org/10.1006/jmsp.1997.7374.